Faculty Publications   Astronomy

2013

Star Formation and Gas Kinematics of Quasar Host Galaxies at z~6: New Insights from ALMA

Ran Wang

Jeff Wagg

Chris L. Carilli

Fabian Walter

Desika Narayanan
Haverford College, dnarayan@haverford.edu

Follow this and additional works at: https://scholarship.haverford.edu/astronomy_facpubs

STAR FORMATION AND GAS KINEMATICS OF QUASAR HOST GALAXIES AT $z \sim 6$: NEW INSIGHTS FROM ALMA

RAN WANG[1,2,14], JEFF WAGG[3], CHRIS L. CARILLI[1], FABIAN WALTER[4], LINDLEY LENTATI[5], XIAOHUI FAN[2],
DOMINIK A. RIECHERS[6], FRANK BERTOLDI[7], DESIKA NARAYANAN[2], MICHAEL A. STRAUSS[8], PIERRE COX[9],
ALAIN OMONT[10], KARL M. MENTEN[11], KIRSTEN K. KNUDSEN[12], ROBERTO NERI[9], AND LINHUA JIANG[13,15]

[1] National Radio Astronomy Observatory, P.O. Box 0, Socorro, NM 87801, USA
[2] Steward Observatory, University of Arizona, 933 North Cherry Avenue, Tucson, AZ 85721, USA
[3] European Southern Observatory, Alonso de Córdova 3107, Vitacura, Casilla 19001, Santiago 19, Chile
[4] Max-Planck-Institute for Astronomy, Königsstuhl 17, D-69117 Heidelberg, Germany
[5] Astrophysics Group, Cavendish Laboratory, JJ Thomson Avenue, Cambridge CB3 0HE, UK
[6] Astronomy Department, Cornell University, 220 Space Sciences Building, Ithaca, NY 14853, USA
[7] Argelander-Institut für Astronomie, University of Bonn, Auf dem Hügel 71, D-53121 Bonn, Germany
[8] Department of Astrophysical Sciences, Princeton University, Princeton, NJ 08544, USA
[9] Institute de Radioastronomie Millimetrique, F-38406 St. Martin d'Heres, France
[10] Institut d'Astrophysique de Paris, CNRS and Université Pierre et Marie Curie, F-75014 Paris, France
[11] Max-Planck-Institut für Radioastronomie, Auf dem Hügel 71, D-53121 Bonn, Germany
[12] Department of Earth and Space Sciences, Chalmers University of Technology, Onsala Space Observatory, SE-43992 Onsala, Sweden
[13] School of Earth and Space Exploration, Arizona State University, Tempe, AZ 85287-1504, USA

ABSTRACT

We present Atacama Large Millimeter/submillimeter Array (ALMA) observations of the [C II] $158\,\mu$m fine structure line and dust continuum emission from the host galaxies of five redshift 6 quasars. We also report complementary observations of 250 GHz dust continuum and CO (6–5) line emission from the $z = 6.00$ quasar SDSS J231038.88+185519.7 using the IRAM facilities. The ALMA observations were carried out in the extended array at $0\rlap{.}''7$ resolution. We have detected the line and dust continuum in all five objects. The derived [C II] line luminosities are 1.6×10^9 to $8.7 \times 10^9\,L_\odot$ and the [C II]-to-FIR luminosity ratios are 2.9–5.1 $\times 10^{-4}$, which is comparable to the values found in other high-redshift quasar-starburst systems and local ultra-luminous infrared galaxies. The sources are marginally resolved and the intrinsic source sizes (major axis FWHM) are constrained to be $0\rlap{.}''3$–$0\rlap{.}''6$ (i.e., 1.7–3.5 kpc) for the [C II] line emission and $0\rlap{.}''2$–$0\rlap{.}''4$ (i.e., 1.2–2.3 kpc) for the continuum. These measurements indicate that there is vigorous star formation over the central few kpc in the quasar host galaxies. The ALMA observations also constrain the dynamical properties of the star-forming gas in the nuclear region. The intensity-weighted velocity maps of three sources show clear velocity gradients. Such velocity gradients are consistent with a rotating, gravitationally bound gas component, although they are not uniquely interpreted as such. Under the simplifying assumption of rotation, the implied dynamical masses within the [C II]-emitting regions are of order 10^{10}–$10^{11}\,M_\odot$. Given these estimates, the mass ratios between the supermassive black holes and the spheroidal bulge are an order of magnitude higher than the mean value found in local spheroidal galaxies, which is in agreement with results from previous CO observations of high redshift quasars.

Key words: galaxies: evolution – galaxies: high-redshift – galaxies: starburst – quasars: general – submillimeter: galaxies

Online-only material: color figures

1. INTRODUCTION

Quasars at redshift 6 and higher provide a unique sample to study the formation of the first supermassive black holes (SMBHs) and their host galaxies at the epoch of cosmic reionization. There are currently more than 60 quasars known at $z \sim 6$, selected from large optical and near-infrared surveys (e.g., the Sloan Digital Sky Survey [SDSS], Fan et al. 2006; Jiang et al. 2008, 2009; the Canada–France High Redshift Quasar Survey, Willott et al. 2007, 2009, 2010; the UKIDSS Large Area Survey [ULAS], Mortlock et al. 2009, 2011; and the Panoramic Survey Telescope and Rapid Response System [Pan-STARRS], Morganson et al. 2012) with optical z-band magnitudes from 18.8 to 24.4 and inferred SMBH masses from 10^8 to a few $10^9\,M_\odot$ (Kurk et al. 2007; Jiang et al. 2007; Willott et al. 2010; De Rosa et al. 2011). The formation of $10^9\,M_\odot$ SMBHs at the

highest redshift suggests fast black hole accretion and significant SMBH-galaxy evolution within 1 Gyr after the big bang (Li et al. 2007; Narayanan et al. 2008; Di Matteo et al. 2012). The co-evolution of the first SMBHs and their host galaxies are studied with observations of dust continuum, molecular CO, and [C II] line emission at submillimeter and millimeter ((sub)mm) wavelengths (e.g., Priddey & McMahon 2001; Walter et al. 2003; Maiolino et al. 2005). Dust heated by the UV photons from young, massive stars presents strong thermal FIR continuum emission. Due to the negative K-correction (Blain & Longair 1993), observations of dust continuum emission at (sub)mm wavelengths provide an efficient way to search for star forming activity at high redshifts (Omont et al. 1996, 2003; Priddey et al. 2003; Bertoldi et al. 2003a; Wang et al. 2007). Molecular gas traced by CO transitions provides the requisite fuel for star formation (Narayanan et al. 2008; Carilli & Walter 2013), and the [C II] $158\,\mu$m fine structure line emission is a principal interstellar coolant, which probes the star forming-powered

photodissociation regions (PDRs) and interstellar medium in these earliest quasar host galaxies (Walter et al. 2009; De Looze et al. 2011; Gallerani et al. 2012; Wagg et al. 2012; Venemans et al. 2012; Carilli & Walter 2013).

Dust and high-order molecular CO line emission in the host galaxies of the $z \sim 6$ quasars have been searched for using the Max Planck Millimeter Bolometer Array (MAMBO) on the IRAM-30 m telescope (Bertoldi et al. 2003a; Petric et al. 2003; Wang et al. 2007, 2008, 2011a; Omont et al. 2013), the Submillimeter Common User Bolometer Array (SCUBA) on the James Clerk Maxwell Telescope (Priddey et al. 2003; Robson et al. 2004; Priddey et al. 2008), and the IRAM Plateau de Bure interferometer (PdBI; Bertoldi et al. 2003b; Walter et al. 2003; Carilli et al. 2007; Wang et al. 2010, 2011a). The MAMBO survey of SDSS $z \sim 6$ quasars at 250 GHz (typical 1σ errors of 0.6 mJy) found that about 30% of them show strong continuum emission from dust at a temperature of 40–60 K, with FIR luminosities of a few 10^{12} to 10^{13} $L_\odot$ and inferred dust masses of a few 10^8 $M_\odot$ (Priddey & McMahon 2001; Bertoldi et al. 2003a; Petric et al. 2003; Wang et al. 2011a). Most of the FIR-luminous $z \sim 6$ quasars also show bright CO line emission, implying that there is $\sim 10^{10}$ $M_\odot$ of molecular gas in the quasar host galaxies (Walter et al. 2003; Carilli et al. 2007; Wang et al. 2010, 2011b). The strong FIR continuum and molecular CO line emission suggest that there is active star formation in the host galaxies of these FIR luminous $z \sim 6$ quasars. The star formation rates inferred from the FIR luminosities range from about a few hundred to one thousand $M_\odot$ yr^{-1} (Bertoldi et al. 2003a; Wang et al. 2008, 2011a).

The CO detections from the FIR-luminous $z \sim 6$ quasars also provide constraints on the spatial distribution of molecular gas and the dynamical masses of the quasar host galaxies (Walter et al. 2004; Wang et al. 2011b). Deep CO line imaging of one of the most FIR-luminous quasars, SDSS J114816.64+525150.3 at $z = 6.42$ (hereafter J1148+5251), using the Very Large Array and the PdBI (Walter et al. 2004; Riechers et al. 2009) at subarcsecond resolution reveals a CO source size of about 3.6 kpc × 1.4 kpc (FWHM) in the central region of the quasar host galaxies. Recent JVLA observations of the CO (2–1) line emission from another FIR-luminous quasar, SDSS J092721.82+200123.7 at $z = 5.77$, at $2''$ resolution has constrained the source size to be about 10 kpc (Wang et al. 2011b). The line widths of the CO-detected $z \sim 6$ quasars range widely from 160 to 860 km s^{-1}. The host galaxy dynamical masses (within the CO emitting region) estimated from the CO line widths and the sizes of the bright detections indicate a median SMBH–bulge mass ratio about one order of magnitude higher than the present-day value (Walter et al. 2004; Wang et al. 2010).

Strong [C II] 158 μm line emission was also detected from the host galaxies of the FIR and CO-luminous quasars at $z \sim 6$ (Maiolino et al. 2005, 2009; Willott et al. 2013). The PdBI image of [C II] line of J1148+5251 shows two components. The narrow-line component with a line width of 345 km s^{-1} and a spatial extension of FWHM $\sim 1''.5$ (8 kpc) traces the distributed star formation in the quasar host galaxy (Maiolino et al. 2012) and the compact core of this component within the central $\sim 0''.3$ region suggests a very high peak star formation rate surface density of ~ 1000 $M_\odot$ yr^{-1} kpc^{-2} (Walter et al. 2009). The broad-line component shows a line width of FWHM ~ 2000 km s^{-1}, distributed over ~ 16 kpc, suggesting gas outflow driven by the central luminous quasar (Maiolino et al. 2012; Valiante et al. 2012). The detection of dust continuum, CO, and [C II] line emission in the quasar host galaxies at $z \sim 6$

suggests an early phase of SMBH-galaxy evolution, in which the SMBHs are accreting at their Eddington limit and the quasar stellar bulges are still accumulating their mass via massive star formation. The interferometer observations of J1148+5251 have demonstrated that the [C II] line emission is an ideal tracer of star-forming activity and gas dynamics in the nuclear region of the starburst quasar host galaxies at the highest redshift.

The Atacama Large Millimeter/submillimeter Array (ALMA) in the early science phase provides a wide frequency coverage for observations of fine structure line emission at high redshift. It also provides the required sensitivity and allows detections of line emission with peak flux density of a few mJy in only one hour of observing time. Additionally, the spatial resolution of $\sim 0''.7$ in Band 6 and 7 in the extended configuration (with a maximum baseline of ~ 400 m) can measure or tightly constrain the distribution of the gas component from high redshift quasar host galaxies. Thus, the Cycle 0 phase of ALMA opens a unique opportunity to expand the observation of [C II] line emission to a large sample of quasar-starburst systems at the highest redshift. In this paper, we present ALMA observations of the [C II] line emission from five FIR luminous quasars at $z \sim 6$. We also report IRAM observations of the 250 GHz dust continuum and CO (6–5) line emission from the quasar SDSS J231038.88+185519.7 at $z = 6.00$ (X. Fan et al. 2013, in preparation). We describe the observations in Section 2, present the results in Section 3, discuss the star forming activity and gas dynamics based on the [C II] line detections in Section 4, and summarize the results in Section 5. A ΛCDM cosmology with $H_0 = 71$ km s^{-1} Mpc^{-1}, $\Omega_M = 0.27$ and $\Omega_\Lambda = 0.73$ is adopted throughout this paper (Spergel et al. 2007).

2. OBSERVATIONS

2.1. IRAM Observations of SDSS J231038.88+185519.7

The quasar SDSS J231038.88+185519.7 (hereafter J2310+ 1855) is a broad absorption line quasar discovered in the SDSS (X. Fan et al. 2013, in preparation). The redshift measured with the quasar rest-frame UV line emission is $z = 6.00 \pm 0.03$. It is one of the optically brightest sources among the known $z \sim 6$ quasars with rest frame 1450 Å magnitude of $m_{1450} = 19.3$. We observed the 250 GHz dust continuum from this object with the MAMBO-II 117-element array on the IRAM 30 m telescope (Kreysa et al. 1998) in the winter of 2010–2011. We adopted the standard on–off photometry mode with a chopping rate of 2 Hz by $32''$ in azimuth. The total observing time was 100 minutes with 50 minutes on source. The data were reduced with the MOPSIC pipeline (Zylka et al. 1998). We reached a 1σ sensitivity of 0.63 mJy and the source is detected at 8.29 mJy ($\sim 13\sigma$), making it the brightest 250 GHz detection among all the known $z \sim 6$ quasars.

We then searched for the CO (6–5) line emission from this object using the PdBI. The observation was carried out in 2011 in D configuration with a synthesized beam size (FWHM) of $5''.4 \times 3''.9$. We spent 3 hr on source using the new wide band correlator WideX, with a bandwidth of 3.6 GHz in dual polarization. The phase was checked with the quasar 3C 454.3 and the flux calibration uncertainty is 5%. The data were reduced with the IRAM GILDAS software package (Guilloteau & Lucas 2000). We detected the line at 11σ with a typical rms of 0.5 mJy beam^{-1} per 100 km s^{-1} channel (Table 1 and Figure 1). We also detected the 99 GHz dust continuum at 8σ with a continuum 1σ sensitivity of 0.05 mJy beam^{-1}.
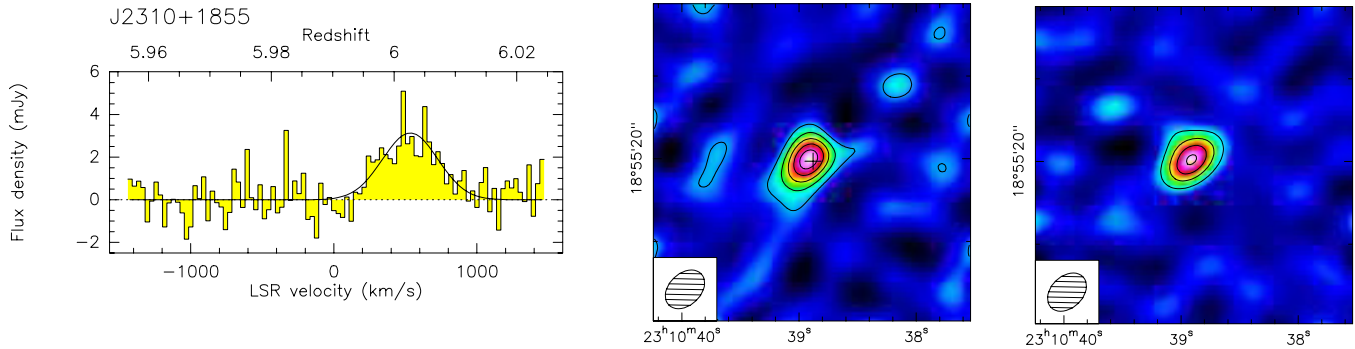
Figure 1. PdBI observation of CO (6–5) line and dust continuum emission at 99 GHz from J2310+1855. The left panel shows the CO (6–5) line spectrum binned to 30 km s^{-1} channels. The solid line is a Gaussian fit to the line spectrum. The middle panel shows the intensity map of the CO (6–5) line emission. The 1σ rms noise of the map is 0.13 Jy km s^{-1} beam^{-1} and the contours in steps of 2σ. The beam size of $5''.4 \times 3''.9$ is plotted on the bottom left. The cross denotes the position of the optical quasar. The right panel is the continuum map at 99 GHz with 1σ rms of 0.05 mJy beam^{-1}, and the contours in steps of 2σ.
(A color version of this figure is available in the online journal.)

Table 1
Summary of Previous Observations

Source	m_{1450}	S_{250} (mJy)	z_{CO}	FWHM$_{CO}$ (km s^{-1})	$S\Delta v_{CO(6-5)}$ (Jy km s^{-1})	$L_{CO(1-0)}$ ($10^5 L_\odot$)
(1)	(2)	(3)	(4)	(5)	(6)	(7)
SDSS J231038.88+185519.7	19.30	8.29 ± 0.63	6.0025 ± 0.0007	456 ± 64	1.52 ± 0.13	32.1
ULAS J131911.29+095051.4	19.65	4.20 ± 0.65	6.1321 ± 0.0012	537 ± 123	0.43 ± 0.09	9.4
SDSS J205406.49−000514.8	20.60	2.38 ± 0.53	6.0379 ± 0.0022	360 ± 110	0.34 ± 0.07	7.3
SDSS J012958.51−003539.7	22.28	2.37 ± 0.49	5.7794 ± 0.0008	283 ± 87	0.37 ± 0.07	7.4
SDSS J104433.04−012502.2	19.21	1.82 ± 0.43	5.7824 ± 0.0007	160 ± 60	0.21 ± 0.04	4.2

Notes. Column 1: name; Column 2: magnitudes at rest-frame 1450 Å (X. Fan et al. 2013, in preparation; Mortlock et al. 2009; Jiang et al. 2008, 2009; Fan et al. 2000); Column 3: continuum flux density at 250 GHz; Columns 4 and 5: redshift and FWHM line width of the CO (6–5) line; Column 6: CO (6–5) line flux of the five objects; Column 7: CO (1–0) line luminosity calculated from the CO (6–5) line emission assuming a CO excitation ladder similar to J1148+5251 (Riechers et al. 2009). The CO (6–5) line measurements for J2310+1855 are from this work, and from Wang et al. (2010, 2011a) for the other four sources.

2.2. ALMA Observations

To study the [C II] 158 μm line emission and the underlying continuum with ALMA, We selected J2310+1855 and another four $z \sim 6$ quasars that were detected in bright millimeter dust continuum and CO (6–5) line emission (Petric et al. 2003; Priddey et al. 2003, 2008; Wang et al. 2008, 2010, 2011a; X. Fan et al. 2013, in preparation) and have declination of $\delta \leqslant +20°$. We list the sources and measurements from previous MAMBO observations in Table 1. The ALMA observations were carried out in Cycle 0 in 2012 with 14–21 12 m diameter antennas in the extended array with baselines from 36 m to 400 m. The typical synthesized beam size (FWHM) is $0''.7$, corresponding to 4 kpc at $z \sim 6$. We observed the [C II] 158 μm (1900.5369 GHz) line emission in Band 6 or 7, with one 2 GHz window centered at the line frequency and the other three 2 GHz windows observing the dust continuum. The correlator channel width is 15.625 MHz, or 16–18 km s^{-1} at the observed line frequency. The phase stability was checked every $\sim$8 minutes by observing nearby phase calibrators (e.g., bright quasars). We spent 50–90 minutes on source for each target and reached 1σ spectral sensitivities of 0.4–0.7 mJy beam^{-1} per 62.5 MHz re-binned channel after continuum subtraction. The continuum sensitivities are 0.04–0.09 mJy beam^{-1} (Table 2).

We reduced the data using the CASA package.[16] The flux scale was calibrated in four of the sources by observing Titan, Neptune, and Uranus, and the calibration uncertainties are better

than 15%. For the source J1044−0125, no primary amplitude calibrator was observed. The flux scale was determined with 3C 273 based on the ALMA and SMA observations in 2012 March and April at 225 GHz and 343 GHz. Considering the uncertainties in the flux densities and spectral index of the calibrator, we estimate a total flux calibration error of 20% for the observation of J1044−0125. We derive the line frequencies in the kinematic local standard of rest frame to compare the results to previous PdBI CO (6–5) line observations.

3. RESULTS

We detected strong [C II] line and dust continuum emission in the host galaxies of all the five $z \sim 6$ quasars. The line emission of the five objects and the continuum emission from four of them (the exception is J1044−0125) are marginally resolved. The line intensity-weighted velocity maps of J0129−0035, J1319+0950, and J2310+1855 show clear velocity gradients (Figure 2). We fit the sizes of the line or continuum sources using the IMFIT task in CASA, which performs synthesized beam deconvolution and two-dimensional (2D) Gaussian fitting to the images. The resulting deconvolved full width at half maximum (FWHM) major axis sizes are $0''.3–0''.6$ (1.7–3.5 kpc) for the line and $0''.2–0''.4$ (1.2–2.3 kpc) for the dust continuum. We list the fitted parameters for each object below. However, we emphasize that, due to the limited spatial resolution, these measurements should be considered as tight constraints on the spatial extent of the sources, rather than accurate source morphology measurements. Interferometer imaging at higher resolution is required to finally
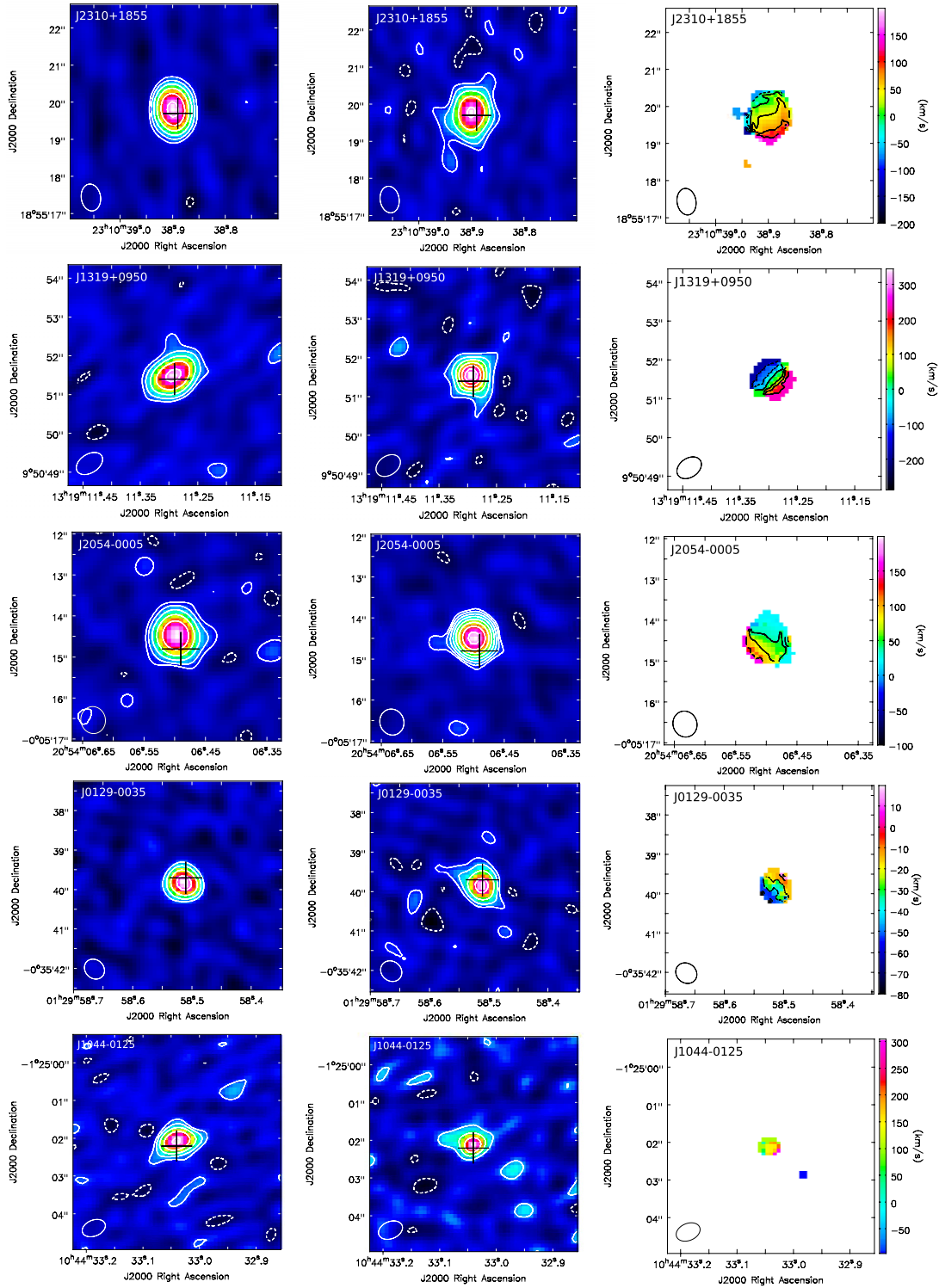
---

[16] http://casa.nrao.edu/

Figure 2. The dust continuum map (left), [C II] line velocity-integrated map (middle), and line velocity maps (right) of the five new [C II] detections. We calculate the line intensity-weighted velocity map using pixels detected at $\geqslant 4\sigma$ in each case. The black crosses show the position of the optical quasar from the discovery paper (X. Fan et al. 2013, in preparation; Mortlock et al. 2009; Jiang et al. 2008, 2009; Fan et al. 2000). The sizes of the synthesized beams are plotted in the bottom-left of each panel. J2310+1855—the continuum contours are $[-2, 2, 4, 8, 32, 64] \times 0.1$ mJy beam^{-1}, and the line contours are $[-2, 2, 4, 8, 16, 32] \times 0.15$ Jy beam^{-1} km s^{-1}. The velocity contours are $[-1, 0, 1, 2, 3] \times 40$ km s^{-1}. The 1σ rms noise is 0.06 mJy beam^{-1} for the continuum map and 0.14 Jy km s^{-1} beam^{-1} for the line map. J1319+0950—the contours are $[-2, 2, 4, 8, 16, 32] \times 0.1$ mJy beam^{-1} for the continuum, $[-2, 2, 4, 6, 8, 10, 12] \times 0.18$ Jy beam^{-1} km s^{-1} for the line, and $[-2, -1, 0, 1, 2, 3] \times 75$ km s^{-1} for the velocity map. The 1σ rms noise values are 0.08 mJy beam^{-1} and 0.18 Jy km s^{-1} beam^{-1} for the continuum and line maps, respectively. J2054−0005—the continuum contours are $[-2, 2, 4, 8, 16, 32, 64] \times 0.04$ mJy beam^{-1}, the line contours are $[-2, 2, 2.83, 4, 5.66, 8, 11.31, 16, 22.63] \times 0.10$ Jy beam^{-1} km s^{-1}, and the contours in the velocity map are $[0, 1, 2] \times 40$ km s^{-1}. The 1σ rms noise is 0.04 mJy beam^{-1} for the continuum map and 0.08 Jy km s^{-1} beam^{-1} for the line map. J0129−0035—the contours are $[-2, 2, 4, 8, 16, 32] \times 0.1$ mJy beam^{-1} for the continuum, $[-2, 2, 4, 8, 16, 32] \times 0.075$ Jy beam^{-1} km s^{-1} for the line, and $[-3, -2, -1, 0] \times 20$ km s^{-1} for the velocity map. The 1σ rms noise is 0.05 mJy beam^{-1} for the continuum map and 0.08 Jy km s^{-1} beam^{-1} for the line map. J1044−0125—the contours are $[-2, 2, 4, 8, 16] \times 0.08$ mJy beam^{-1} for the continuum and $[-2, 2, 4, 6, 8] \times 0.14$ Jy beam^{-1} km s^{-1} for the line. The 1σ rms noise is 0.09 mJy beam^{-1} for the continuum map and 0.14 Jy km s^{-1} beam^{-1} for the line map. The zero velocity in the velocity maps corresponds to the CO redshifts listed in Table 1.

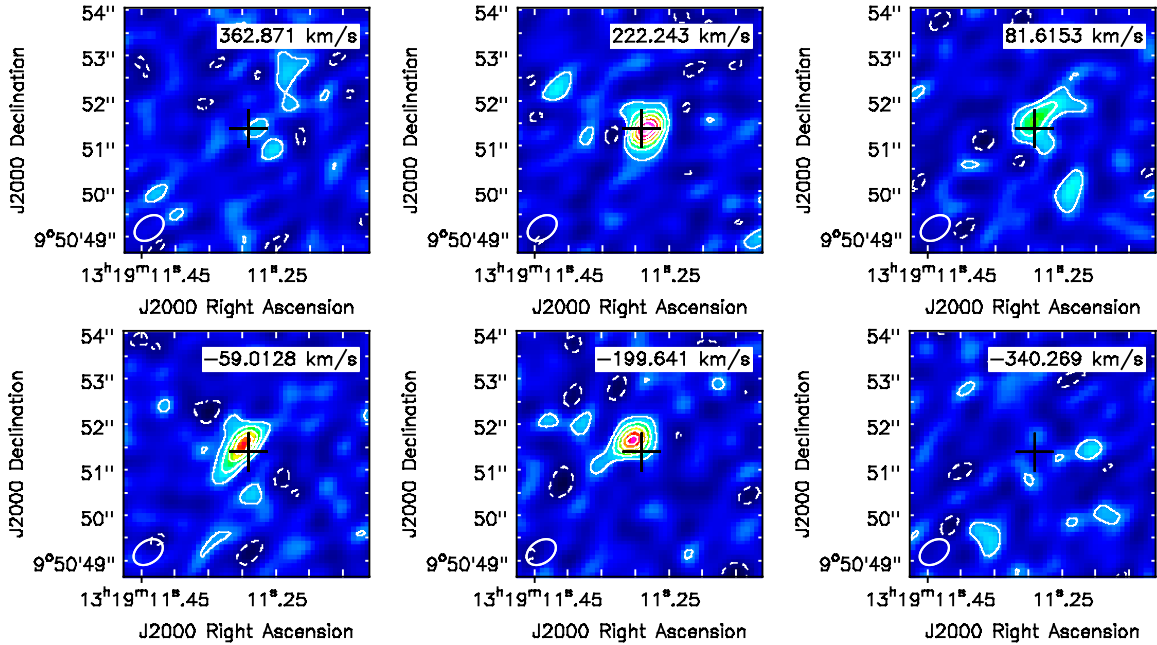(A color version of this figure is available in the online journal.)

Figure 3. [C II] line channel maps of J1319+0950 in the velocity range of −340.3 to +362.9 km s^{-1} at 0″.7 × 0″.5 resolution. The channel width is 140 km s^{-1} for each map, and the line is clearly detected in the middle four channels. The typical 1σ rms noise of the channel map is 0.54 mJy beam^{-1}, and the contours are [−2, 2, 4, 6, 8, 10, 12] × 1σ. The peak of the [C II] line emission is shifted by about 0″.4 from the 222 km s^{-1} channel to the −200 km s^{-1} channel. The cross denotes the location of the optical quasar.

(A color version of this figure is available in the online journal.)

Table 2
ALMA Observations

Source	t_{on} (min)	$z_{[C II]}$	$S\Delta v$ (Jy km s^{-1})	FWHM$_{[C II]}$ (km s^{-1})	rms$_{[C II]}$ (mJy beam^{-1})	ν_{con} (GHz)	S_{con} (mJy)	rms$_{con}$ (mJy beam^{-1})
(1)	(2)	(3)	(4)	(5)	(6)	(7)	(8)	(9)
J2310+1855	50	6.0031 ± 0.0002	8.83 ± 0.44	393 ± 21	0.5	263	8.91 ± 0.08	0.06
J1319+0950	80	6.1330 ± 0.0007	4.34 ± 0.60	515 ± 81	0.7	258	5.23 ± 0.10	0.08
J2054−0005	40	6.0391 ± 0.0001	3.37 ± 0.12	243 ± 10	0.4	262	2.98 ± 0.05	0.04
J0129−0035	60	5.7787 ± 0.0001	1.99 ± 0.12	194 ± 12	0.4	287	2.57 ± 0.06	0.05
J1044−0125	87	5.7847 ± 0.0007	1.70 ± 0.30	420 ± 80	0.6	287	3.12 ± 0.09	0.09

Notes. Column 1: source; Column 2: on-source time of the ALMA [C II] observations; Columns 3–5: redshift, flux, and FWHM line width of the [C II] line fitted to a single Gaussian line profile; Column 6: ALMA 1σ line sensitivity bin to a channel width of 62.5 MHz (∼70 km s^{-1}); Columns 7 and 8: frequency and flux density of the continuum measured with the line-free windows; Column 9: ALMA 1σ rms continuum sensitivity integrated over a total bandwidth of 5.8–6 GHz. The flux errors quoted here are from our fitting process described in Section 3. The calibration uncertainties are not included here.

determine the source morphology. To measure the line center, FWHM line width, and flux, we subtract the underlying dust continuum in the $U − V$ plane, calculate the line spectra by integrating the intensity over the line-emitting region in each channel, and fit the spectra with a Gaussian profile. The [C II] results are summarized in Table 2, and the line and continuum maps are presented in Figures 2 and 3.

SDSS J2310+1855. This object is the brightest detection among all the $z \sim 6$ quasars from our MAMBO observations. The 250 GHz continuum flux density is 8.29 ± 0.63 mJy. Our PdBI observation of the CO(6–5) line emission shows a line flux of 1.52 ± 0.13 Jy km s^{-1}, which is also by far the strongest CO line flux. The redshift and FWHM measured with the CO (6–5) line are $z_{CO} = 6.0025 ± 0.0007$ and FWHM$_{CO} = 456 ± 64$ km s^{-1}. The dust continuum at 99 GHz has also been detected in the line-free channels with a flux density of 0.40 ± 0.05 mJy (Figure 1).

We detect the [C II] line emission with a flux which is again more than twice stronger than the four other sources. The derived FWHM source size, after deconvolving the 0″.72 × 0″.51

synthesized beam, is (0″.56 ± 0″.03) × (0″.39 ± 0″.04) with a position angle (P.A.) of 142° ± 10° east of north. The line intensity-weighted velocity map derived with the line-emitting channels indicates a velocity gradient from southwest to northeast (see the right panels of Figure 2). The 263 GHz continuum flux density imaged with the line-free windows and fitted to a 2D Gaussian is 8.91 ± 0.08 mJy, which is in very good agreement with the MAMBO value. This constrains the (deconvolved) continuum source size to be (0″.25 ± 0″.02) × (0″.20 ± 0″.02) with P.A. = 162° ± 18°.

J1319+0950. This quasar was discovered in the UKIRT Infrared Deep Sky Survey (UKIDSS) and has $m_{1450} = 19.65$ (Mortlock et al. 2009). The [C II] line emission is imaged by ALMA with a synthesized beam size of 0″.69 × 0″.49. The 2D Gaussian fit suggests line emission with a deconvolved source size of (0″.57 ± 0″.07) × (0″.32 ± 0″.15) oriented at P.A. = 28° ± 18°. The line velocity map shows a clear gradient from the southwest to the northeast. We plot the [C II] line channel map of this object in Figure 3. The map shows a clear position shift of the [C II] line peak (by ∼0″.4) from the

Table 3
Luminosities and Dynamical Masses

Source	$L_{[C II]}$ $(10^9 L_\odot)$	L_{FIR} $(10^{12} L_\odot)$	L_{bol} $(10^{13} L_\odot)$	M_{BH} $(10^9 M_\odot)$	$M_{dyn}\sin^2 i$ $(10^{10} M_\odot)$	M_{dyn} $(10^{10} M_\odot)$	M_{BH}/M_{dyn}
(1)	(2)	(3)	(4)	(5)	(6)	(7)	(8)
J2310+1855	8.7 ± 1.4	17.0 ± 1.8	9.3	2.8	4.9 ± 0.6	9.6	0.030
J1319+0950	4.4 ± 0.9	10.7 ± 1.3	7.0	2.1	8.5 ± 2.9	12.5	0.017
J2054−0005	3.3 ± 0.5	8.0 ± 3.3	2.8	0.86	1.2 ± 0.2	7.2	0.012
J0129−0035	1.8 ± 0.3	4.6 ± 0.6	0.57	0.17	0.9 ± 0.2	1.3	0.013
J1044−0125	1.6 ± 0.4	5.5 ± 0.7	11.6	10.5	. . .	. . .	. . .

Notes. Column 1: source; Column 2: [C II] line luminosity; Column 3: FIR luminosity in the wavelength range from 42.5 μm to 122.5 μm (see Section 3 for details). We considered both measurement errors listed in Table 2 and the 15%–20% calibration uncertainties in the calculation of $L_{[C II]}$ and L_{FIR}. Column 4: quasar bolometric luminosities. The bolometric luminosity for J1044−0125 is taken from Jiang et al. (2006), and we estimate the bolometric luminosities for the other four objects from their rest-frame 1450 Å magnitude, assuming an isotropic bolometric correction of $L_{bol} = 4.2L_{1450}$ (Runnoe et al. 2012a, 2012b); Column 5: SMBH masses. The SMBH mass of J1044−0125 is calculated from the quasar C IV line emission (Jiang et al. 2007), and we estimate the SMBH masses for the other four sources from the bolometric luminosities assuming Eddington accretion; Column 6: dynamical mass without inclination angle correction, estimated from the [C II] line width and source size (see Section 4.2); Column 7: inclination angle-corrected dynamical mass within the [C II]-emitting region. We estimate the disk inclination angle from the [C II] minor and major axis ratio as $i = 46°$, $56°$, $24°$, and $56°$ for J2310+1855, J1319+0950, J2054−0005, and J0129−0035, respectively; Column 8: SMBH–bulge mass ratio.

+222 km s^{-1} channel to the −200 km s^{-1} channel. The 258 GHz continuum flux density is 5.23 ± 0.10 mJy and the deconvolved continuum source size is $(0.39 \pm 0.02) \times (0.34 \pm 0.03)$ with P.A. $= 121° \pm 148°$.

J2054−0005. The quasar was selected from SDSS stripe 82 with $m_{1450} = 20.60$, i.e., about one magnitude fainter than the objects discovered from the SDSS main survey (Jiang et al. 2008). We observed the [C II] line emission at 0.64×0.58 resolution. The deconvolved FWHM source size is $(0.35 \pm 0.04) \times (0.32 \pm 0.05)$ and P.A. $= 91° \pm 173°$. The 262 GHz continuum flux density measured in the line-free windows is 2.98 ± 0.05 mJy, and the deconvolved continuum source size is $(0.27 \pm 0.03) \times (0.26 \pm 0.03)$ with P.A. $= 168° \pm 68°$.

J0129−0035. This quasar was discovered in SDSS stripe 82 with $m_{1450} = 22.16$ (Jiang et al. 2009). It is the faintest optical source among the MAMBO-detected $z \sim 6$ quasars, but previous millimeter observations found bright 250 GHz dust continuum and CO (6–5) line emission from this object (Wang et al. 2011a). The [C II] line was observed at 0.57×0.49 resolution. The deconvolved source size is estimated to be $(0.41 \pm 0.06) \times (0.23 \pm 0.12)$ with P.A. $= 12° \pm 22°$. A velocity gradient is found from the southeast to the northwest. A 2D Gaussian fit to the continuum image gives a 287 GHz flux density of 2.57 ± 0.06 mJy, with a deconvolved continuum source size of $(0.23 \pm 0.04) \times (0.14 \pm 0.07)$ at P.A. $= 115° \pm 154°$.

J1044−0125. This is another broad absorption line quasar at $z \sim 6$ discovered from the SDSS main survey with $m_{1450} = 19.2$ (Fan et al. 2000). A deep near-IR spectrum of the quasar C IV line emission of this object yields a SMBH mass of $10.5 \times 10^9 M_\odot$ (Jiang et al. 2007). The beam size of the [C II] line observation is 0.66×0.45 and the deconvolved source size is estimated to be $(0.61 \pm 0.11) \times (0.33 \pm 0.22)$ oriented at P.A. $= 65° \pm 48°$. No gradient is seen in the line intensity-weighted velocity map of this object. The 287 GHz continuum flux density is 3.12 ± 0.09 mJy and the source is unresolved in the continuum.

We calculate the [C II] line luminosity of each source as $L_{[C II]}/L_\odot = 1.04 \times 10^{-3} S\Delta v \nu_0 (1 + z)^{-1} D_L^2$ (Solomon & Vanden Bout 2005), where $\nu_0 = 1900.5369$ GHz is the rest frame [C II] line frequency, $S\Delta v$ is the integrated line flux in Jy km s^{-1}, and D_L is the luminosity distance in Mpc. The derived

line luminosities are in the range of 1.6–8.7 $\times 10^9 L_\odot$. We also calculate the CO (6–5) line luminosity for J2310+1855, which is $(5.4 \pm 0.5) \times 10^8 L_\odot$ or $(5.1 \pm 0.4) \times 10^{10}$ K km s^{-1} pc^2.

We then estimate their FIR luminosities (L_{FIR}) by fitting a modified blackbody (i.e., $S_\nu \sim \nu^{3+\beta}/(\exp(h\nu/kT_{dust}) - 1)$; Priddey & McMahon 2001; De Breuck et al. 2003; Kovács et al. 2006) to the ALMA continuum flux densities, MAMBO (Petric et al. 2003; Wang et al. 2007, 2008, 2011a), and available PdBI and SCUBA data (Priddey et al. 2003, 2008; Wang et al. 2010, 2011a). For four of the five objects (except J2054−0005), we adopt a dust temperature of $T_{dust} = 47$ K and emissivity index of $\beta = 1.6$, which are the mean values found in the sample of high-z FIR luminous quasars (Beelen et al. 2006). This yields the FIR luminosities (L_{FIR}) in the range 42.5–122.5 μm of 5–17 $\times 10^{12} L_\odot$.[17] The estimates of L_{FIR} could be larger by up to 20% if a higher dust temperature of 50 K is assumed, or lower by $\leqslant 8\%$ if the best fit of $z > 4$ quasars from Priddey & McMahon (2001; i.e., $T_{dust} = 41$ K and $\beta = 1.95$) is adopted. J2054−0005 was recently detected by *Herschel*/SPIRE at 250 μm and 350 μm, which samples the continuum at wavelengths close to or shorter than the peak of the starburst-powered thermal dust emission (Leipski et al. 2013). As the 250 μm flux density might be significantly contaminated by the emission from the active galactic nucleus (AGN) dust torus (Leipski et al. 2013), we fit L_{FIR} for this object with the *Herschel* 350 μm, the MAMBO 250 GHz, and ALMA 262 GHz measurements, and leave T_{dust} as a free parameter. The fit suggests $T_{dust} = 52 \pm 6$ K and $L_{FIR} = (8.0 \pm 3.3) \times 10^{12} L_\odot$. We have listed the derived [C II] and FIR luminosities in Table 3.

4. DISCUSSION

4.1. Distributions of Gas, Dust, and Star Formation in the Quasar Host Galaxies

The new detections of strong [C II] line emission toward the five FIR-luminous quasars at $z \sim 6$ provide further evidence for active star formation in the quasar host galaxies. The [C II]

---

[17] Based on the modified blackbody model (i.e., $T_{dust} \sim 47$ K, $\beta \sim 1.6$, Beelen et al. 2006), the commonly used infrared luminosity integrated from 8 to 1000 μm is about 1.4 times larger than the 42.5–122.5 μm FIR luminosity we used here.

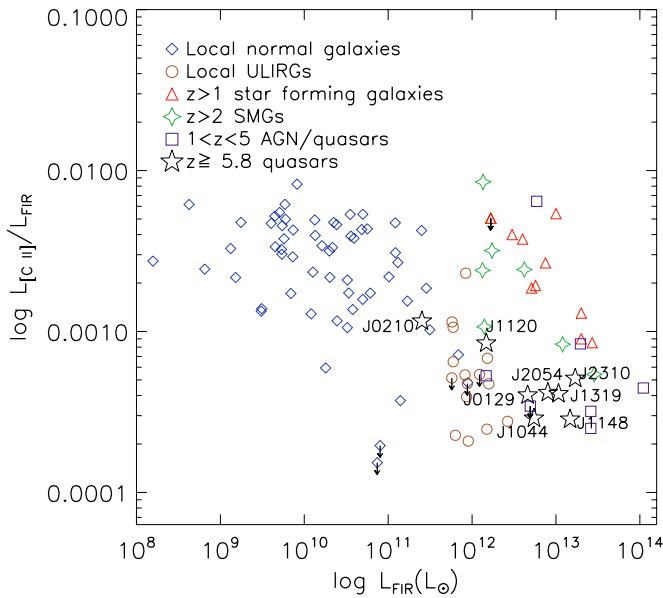**Figure 4.** $L_{[C II]}/L_{FIR}$ vs. L_{FIR}. The black stars indicate the quasars at $z \geqslant 5.8$, including the five new [C II]-detected $z \sim 6$ quasars in this work, J1148+5251 at $z = 6.42$ (Maiolino et al. 2005; Leipski et al. 2013), CFHQS J0210−0456 at $z = 6.43$ (Willott et al. 2013), and the $z = 7.08$ quasar ULAS J112001.48+064124.3 (Venemans et al. 2012). We also plot the luminosity ratios from samples of local normal star forming galaxies (Malhotra et al. 2001), ULIRGs (Luhman et al. 2003), $z > 1$ star forming galaxies and mixed systems (Stacey et al. 2010; Marsden et al. 2005), $z > 2$ submillimeter bright galaxies (SMG; Maiolino et al. 2009; Ivison et al. 2010; De Breuck et al. 2011; Swinbank et al. 2012; Wagg et al. 2012; Valtchanov et al. 2011; Riechers et al. 2013), and $1 < z < 5$ [C II] detected quasars (Pety et al. 2004; Maiolino et al. 2005, 2009; Gallerani et al. 2012; Wagg et al. 2012; Carilli et al. 2013) for comparison.

line emission is marginally resolved in all these objects. The ALMA observations at $0\farcs7$ resolution yield estimates of the intrinsic [C II] source sizes (FWHM of the major axis) of $0\farcs3$–$0\farcs6$ (1.7–3.5 kpc). Clear velocity gradients have been found in the line intensity-weighted velocity maps of J2310+1855, J1319+0950, and J0129−0035, which suggests that the gas could be in rotation, and gravitationally bound, e.g., a non-face-on rotating disk. The dust continuum flux densities measured in the vicinity of the [C II] line frequencies for all five objects are consistent with previous MAMBO measurements at 250 GHz. The continuum sources of four of them (except J1044−0125) are marginally resolved, indicating deconvolved FWHM major axis sizes of $0\farcs2$–$0\farcs4$, or 1.2–2.3 kpc. These results constrain the spatial extent of star forming activity to be 2.6–5.3 kpc in diameter[18] in the nuclear region. We will observe these sources with ALMA in Cycle 1 at $0\farcs2$ resolution to fully resolve the line and dust continuum sources, and measure what fraction of the dust continuum emission is from the central compact AGN. These observations will finally measure the star formation rates (SFR) and SFR surface densities in these earliest quasar-starburst systems. The higher resolution imaging will also address if the gas components in the nuclear starburst region are uncoalesced and show multiple-peak morphology in line emission (Walter et al. 2004), which was suggested by the galaxy merger models of quasar-galaxy formation (e.g., Narayanan et al. 2008)

In Figure 4, we plot the [C II]-to-FIR luminosity ratios of the [C II]-detected $z \geqslant 5.8$ quasars, including the five new

detections in this work, J1148+5251 (Maiolino et al. 2005), CFHQS J0210−0456 at $z = 6.43$ (Willott et al. 2013), and ULAS J1120+0640 at $z = 7.08$ (Venemans et al. 2012). We compare them to samples of [C II]-detected local normal star forming galaxies, ULIRGs, submillimeter galaxies, and FIR-luminous quasars at high redshift (Malhotra et al. 2001; Luhman et al. 2003; Stacey et al. 2010; Maiolino et al. 2009; Ivison et al. 2010; De Breuck et al. 2011; Swinbank et al. 2012; Wagg et al. 2012; Pety et al. 2004; Gallerani et al. 2012; Carilli et al. 2013; Valtchanov et al. 2011; Riechers et al. 2013; Marsden et al. 2005). The five $z \sim 6$ quasars presented in this work, as well as J1148+5251, show luminosity ratios of 2.9–5.1×10^{-4}, which are comparable to the typical values found in local ULIRGs and $1 \leqslant z \leqslant 5$ [C II]-detected quasars, and a few to 10 times lower than that of the disk star forming galaxies and submillimeter galaxies. We also notice that the other two $z > 6$ quasars with moderate FIR luminosities (10^{11}–$10^{12} L_\odot$) show higher $L_{[C II]}/L_{FIR}$ than most FIR luminous objects (Venemans et al. 2012; Willott et al. 2013). We estimate the CO (1–0) line luminosities for the five objects from the PdBI CO (6–5) detections (last column of Table 1), assuming a CO excitation ladder similar to J1148+5251 (Riechers et al. 2009). The calculated [C II]-to-CO (1–0) line luminosity ratios are about 2400–4700, which is slightly higher than the values found in local ULIRGs (Luhman et al. 2003), and the highest value is close to the median luminosity ratios found in starburst galaxies (i.e., $L_{[C II]}/L_{CO} \sim 4400$; Stacey et al. 1991, 2010; Swinbank et al. 2012).

The [C II], FIR, and CO luminosity ratios of the five [C II]-detected $z \sim 6$ quasars can be reproduced by PDR models (Kaufman et al. 1999; Stacey et al. 2010; Luhman et al. 2003) with gas density on orders of 10^4–10^5 cm^{-3} and FUV (6 eV $< h\nu <$ 13.6 eV) radiation field G_0 of a few 10^3–10^4 (in units of the Habing Field, 1.6×10^{-3} erg cm^{-2} s^{-1}; Kaufman et al. 1999). However, such strong radiation fields will also produce strong [O I] 63 μm line emission with intensities comparable or higher than the [C II] line (Kaufman et al. 1999; Luhman et al. 2003; Carilli et al. 2013). Thus future observations of the [O I] and other fine structure lines from these objects with the full configuration of ALMA will be a crucial test of the physical conditions inferred from these PDR models. It is also possible that the central AGN has substantial contribution to the dust heating and FIR emission, which results in lower [C II]-to-FIR luminosity ratios in the nuclear region (Luhman et al. 2003; Sargsyan et al. 2012).

We compare the [C II] and CO (6–5) line profiles of the five objects in Figure 5. For four of the five sources, the redshifts measured with [C II] and CO (6–5) are consistent within the 1σ errors; there are no large velocity offsets between the gas components traced by [C II] and CO (6–5) lines. The [C II] FWHM line widths of J2310+1855, J2054−0005, and J0129−0035 are about 60 to 115 km s^{-1} smaller than the CO (6–5) measurements. But these differences are within the 1σ–2σ error bars, as the CO (6–5) line width uncertainties for these objects are between 60 and 120 km s^{-1} (Table 1). The other object, J1044−0125, shows a larger [C II] redshift with $\Delta z = z_{[C II]} - z_{CO} = 0.0023 \pm 0.0010$ (i.e., a velocity difference of 100 ± 44 km s^{-1}), and a much broader [C II] line width (Figure 5). This may indicate different kinematical properties between the two gas components in this object. However, it is also possible that a large fraction of the CO line emission is undetected and the CO line width is underestimated due to the low signal-to-noise ratio of the line spectrum. Thus, deep

---

[18] We adopt a source size of $1.5\times$ the FWHM major axis from the [C II] intensity map (i.e., full width at 20% of the peak intensity for a Gaussian profile).
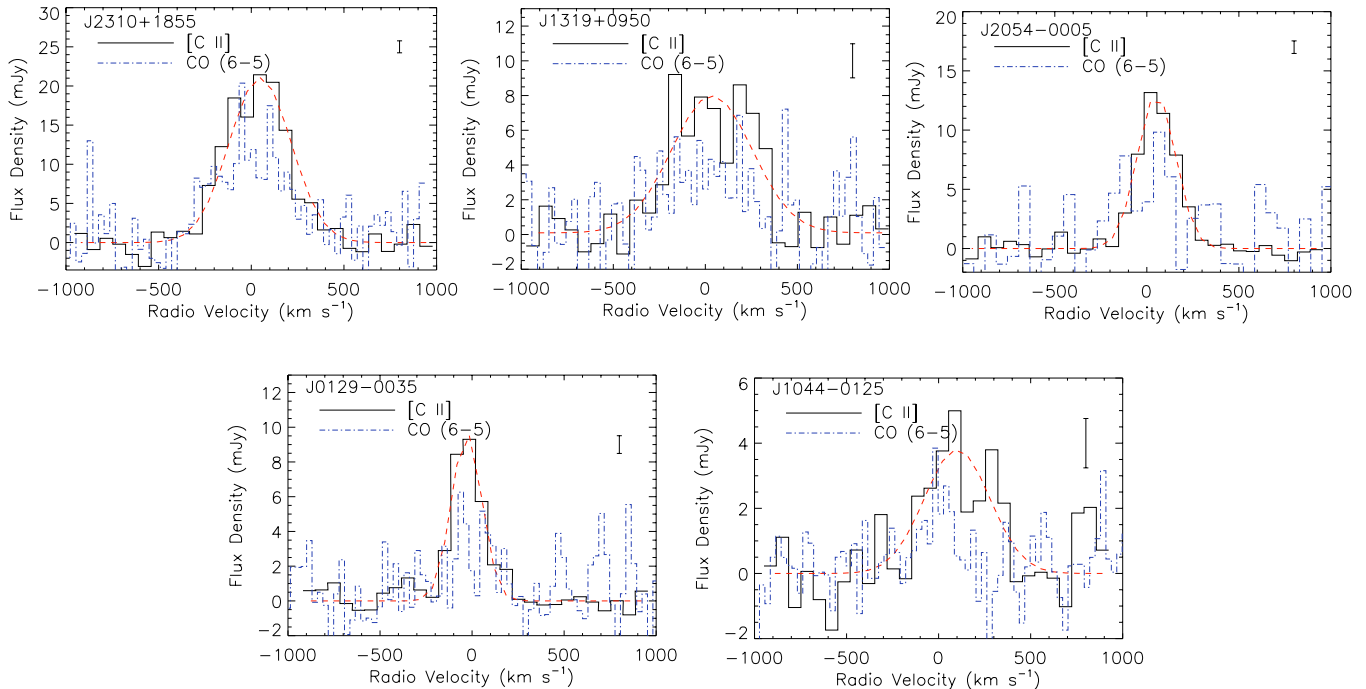
Figure 5. The [C II] line spectra (black solid line) of the five ALMA detected quasars integrated over the line-emitting region in each channel, together with the previous CO (6–5) detections from PdBI (blue dotted line, scaled to the [C II] line) and a Gaussian fit to the [C II] line (red dashed line). The typical $\pm 1\sigma$ error per channel for the [C II] line spectrum is shown in the top right of each panel. The zero velocity corresponds to the CO redshift listed in Table 1.
(A color version of this figure is available in the online journal.)

imaging of the CO line emission with better measurements of the CO line profile and spatial distribution is needed to address whether the [C II]-emitting gas is more centrally concentrated in J2310+1855, J2054−0005, and J0129−0035, and to understand the origin of the narrower CO line in J1044−0125.

4.2. Dynamical Masses Traced by the [C II] Line Emission

If we assume a rotating disk geometry for the [C II]-emitting gas in these FIR-luminous $z \sim 6$ quasars,[19] we can estimate the dynamical masses within the [C II]-emitting regions for J2310+1855, J1319+0955, J2054−0005, and J0129−0035 as $M_{dyn}/M_\odot \approx 1.16 \times 10^5 v_{cir}^2 D$, where D is the disk diameter in kpc from the [C II] measurements (2.6–5.3 kpc; see Section 4.1) and v_{cir} is the maximum circular velocity of the gas disk in km s^{-1}. We estimate v_{cir} as $v_{cir} = 0.75 \text{FWHM}_{[C II]}/\sin i$ (i.e., half width at 20% line maximum), where i is the inclination angle between the gas disk and the line of sight ($i = 0°$ for a face-on disk). The derived $M_{dyn}\sin^2 i$ are 0.9–8.5 $\times 10^{10}$ $M_\odot$, and the uncertainties estimated with the measurement errors in $\text{FWHM}_{[C II]}$ and [C II] source size are about 10%–40%. With the assumption of an inclined disk geometry, we can also have a first guess at the disk inclination angle from the [C II] minor and major axis ratios (R), i.e., $i = \cos^{-1}(R)$, though we should keep in mind that the source size measurements at current spatial resolution ($\sim 0\rlap{.}''7$) still have large uncertainties (see Section 3). The estimated inclination angles are 46°, 56°, 24°, and 56° for J2310+1855, J1319+0955, J2054−0005, and J0129−0035, respectively. This gives inclination angle-corrected dynamical masses of $M_{dyn} = 1.3 \times 10^{10}$ to 1.2×10^{11} $M_\odot$. We list the derived inclination angle-corrected dynamical mass M_{dyn} in Table 3.

---

[19] We exclude J1044−0125 in the discussion here as the difference between the [C II] and CO (6–5) line spectra may indicate more complicated gas dynamics.

There are no published SMBH masses for the four objects yet. We calculate the 1 μm to 8 keV quasar bolometric luminosities for the four sources using an isotropic bolometric correction of $L_{bol} = 4.2L_{1450}$ (Runnoe et al. 2012a, 2012b), where L_{1450} is the rest-frame 1450 Å luminosity calculated from the 1450 Å magnitudes in the discovery papers (Fan et al. 2000, 2006; Jiang et al. 2009; Mortlock et al. 2009; X. Fan et al. 2013, in preparation). We here assume that the dust extinction from quasar host galaxies at 1450 Å is negligible. We then derive the SMBH masses (M_{BH}) from the quasar luminosity assuming Eddington accretion. The resulting mass ratios M_{BH}/M_{dyn} lie in the range of 0.012–0.030 (see Table 3). Note that the M_{BH} and M_{BH}/M_{dyn} values could be even larger if the typical ratio between quasar bolometric luminosity and Eddington luminosity is less than unity (e.g., De Breuck et al. 2011) or the 1450 Å luminosities are obscured by the dust in the quasar host galaxies (Maiolino et al. 2004; Gallerani et al. 2010; Hjorth et al. 2013).

The [C II]-based M_{BH}/M_{dyn} values are consistent with the previous CO estimates of the median SMBH–bulge mass ratio of these $z \sim 6$ quasars (Wang et al. 2010) and agree with the results found with other high-z FIR and CO luminous quasars that the SMBH–bulge mass ratios are 10–30 times higher than the average value of 0.0014 found in local normal galaxies (Marconi et al. 2003; Walter et al. 2004; Riechers et al. 2008; Wang et al. 2010; Coppin et al. 2008; Venemans et al. 2012). However, one should be cautious with these [C II]-based M_{dyn} values, as the detected [C II] line emission may trace only the intense star forming region in the very centers of quasar host galaxies and not extend as far as the stellar bulge. This may underestimate the total masses within the spheroidal stellar bulges. Additionally, we notice that there are still large uncertainties in the intrinsic source morphology measurements; the deconvolved minor axis and position angle measurements

of some of the objects show large error bars. This can introduce significant uncertainties in the inclination and dynamical mass estimate. Further ALMA imaging of these FIR-luminous $z \sim 6$ quasars at $\lesssim 0\rlap{.}''2$ will be crucial to better constrain the distribution and dynamical properties of the gas components, address how well the atomic/molecular line emission traces the dynamical masses of the quasar host galaxies, and determine whether the high M_{BH}/M_{dyn} ratio is common in the massive quasar-starburst systems in the early universe.

4.3. Search for [C II] Line Emitters Associated with the Quasar Environments

Given the sensitivity of the ALMA Band 6 and Band 7 data, and the large spectral bandwidth (7.5 GHz, or ~ 9000 km s^{-1}), it is plausible that serendipitous line emission from companion objects will be detected in our data. Although the volume is relatively small over the five fields (each field was observed across four 1.875 GHz spectral windows, covering a redshift range $\Delta z \sim 0.2$ which, for a primary beam with FWHM $\sim 22''$, results in a total surveyed volume of ~ 280 Mpc^3), recent ALMA surveys of submm luminous starburst galaxies at $z \sim 4.4$ suggest a strong evolution in the [C II] luminosity function out to these early cosmic times (Swinbank et al. 2012). We use a Bayesian search algorithm developed to efficiently search for broad, weak line emission in large spectral line data cubes (Lentati et al. 2013), and use the evidence for candidate detections to calculate the probability that detected candidates are "real" relative to being noise. We do not find any candidate detections of serendipitous line emission in our data with probabilities above 25%. At the current sensitivity the volume sampled is not sufficient to place constraints on the possible evolution of the luminosity function out to $z \sim 6$, with source counts (i.e., 10^{-3} Mpc^{-3}; Swinbank et al. 2012) derived from the [C II] luminosity function predicting ~ 0.3 detection above a 3σ luminosity limit $L_{[C II]} > 2.1 \times 10^8 \, L_\odot$. However the sensitivity of ALMA at bands 6 and 7 means that deeper observations in Cycle 1 of similar volumes will allow us to place strong constraints on the obscured star-formation properties of galaxies in the environments of the quasars.

5. SUMMARY

We detected [C II] fine structure line and dust continuum emission from the host galaxies of five quasars at $z \sim 6$, using ALMA in the Cycle 0 phase at $\sim 0\rlap{.}''7$ resolution. Complementary IRAM observations of the CO (6–5) line and 250 GHz dust continuum emission from the $z = 6.00$ quasar J2310+1855 are also presented. Our ALMA observations measure the FWHM major axis sizes of the [C II] emission from the five objects to be $0\rlap{.}''3$–$0\rlap{.}''6$ (1.7–3.5 kpc) and the sizes of the dust continuum source for four of them to be $0\rlap{.}''2$–$0\rlap{.}''4$ (1.2–2.3 kpc). The detections of [C II] line and dust continuum emission indicate active star formation in the central few kpc region of the quasar host galaxies. The derived [C II]-to-FIR luminosity ratios are of the order 10^{-4}, which are comparable to the typical values found in local ULIRGs and other FIR-luminous quasars at high redshift. The intensity-weighted velocity maps of J2310+1855, J1319+0950, and J0129−0035 show velocity gradients. Such velocity gradients are consistent with rotation, although they are not uniquely interpreted as such. We estimate the dynamical masses within the [C II]-emitting region for four of the five objects assuming that the gas is distributed in a rotating disk. The derived ratios between the SMBH masses and the dynamical

masses are one order of magnitude higher than that of local normal galaxies.

The detections of [C II] 158 μm line emission from quasar host galaxies at $z \sim 6$ have demonstrated the power of ALMA in observing signatures of star formation at the earliest cosmic epoch. With the full configuration of ALMA, we should be able to resolve the line and dust continuum emission on kpc or sub-kpc scales, which will measure the surface densities of the gas components and star forming activity in the nuclear region, and better address the gas kinetics and dynamical masses of the spheroidal quasar host galaxies. The full frequency coverage of ALMA will also allow a search of other ionized/atomic interstellar cooling lines from these FIR-luminous $z \sim 6$ quasars to measure the physical conditions (e.g., density, radiation field, temperature, etc.) of the interstellar medium in these earliest quasar-starburst systems.

REFERENCES

Beelen, A., Cox, P., Benford, D. J., et al. 2006, ApJ, 642, 694
Bertoldi, F., Carilli, C. L., Cox, P., et al. 2003a, A&A, 406, L55
Bertoldi, F., Cox, P., Neri, R., et al. 2003b, A&A, 409, L47
Blain, A. W., & Longair, M. S. 1993, MNRAS, 264, 509
Carilli, C. L., Neri, R., Wang, R., et al. 2007, ApJL, 666, L9
Carilli, C. L., Riechers, D., Walter, F., et al. 2013, ApJ, 763, 120
Carilli, C. L., & Walter, F. 2013, ARA&A, 51, in press (arXiv:1301.0371)
Coppin, K. E. K., Swinbank, A. M., Neri, R., et al. 2008, MNRAS, 389, 45
De Breuck, C., Maiolino, R., Caselli, P., et al. 2011, A&A, 530, L8
De Breuck, C., Neri, R., Morganti, R., et al. 2003, A&A, 401, 911
De Looze, I., Baes, M., Bendo, G. J., Cortese, L., & Fritz, J. 2011, MNRAS, 416, 2712
De Rosa, G., Decarli, R., Walter, F., et al. 2011, ApJ, 739, 56
Di Matteo, T., Khandai, N., DeGraf, C., et al. 2012, ApJL, 745, L29
Fan, X., Strauss, M. A., Richards, G. T., et al. 2006, AJ, 131, 1203
Fan, X., White, R. L., Davis, M., et al. 2000, AJ, 120, 1167
Gallerani, S., Maiolino, R., Juarez, Y., et al. 2010, A&A, 523, 85
Gallerani, S., Neri, R., Maiolino, R., et al. 2012, A&A, 543, 114
Guilloteau, S., & Lucas, R. 2000, ASPC, 217, 299
Hjorth, J., Vreeswijk, P. M., Gall, C., & Watson, D. 2013, ApJ, 768, 173
Ivison, R. J., Swinbank, A. M., Swinyard, B., et al. 2010, A&A, 518, L35
Jiang, L., Fan, X., Annis, J., et al. 2008, AJ, 135, 1057
Jiang, L., Fan, X., Bian, F., et al. 2009, AJ, 138, 305

Jiang, L., Fan, X., Hines, D. C., et al. 2006, AJ, 132, 2127
Jiang, L., Fan, X., Vestergaard, M., et al. 2007, AJ, 134, 1150
Kaufman, M. J., Wolfier, M. G., Hollenbach, D. J., & Luhman, M. L. 1999, ApJ, 527, 795
Kovács, A., Chapman, S. C., Dowell, C. D., et al. 2006, ApJ, 650, 592
Kreysa, E., Gemuend, H., Gromke, J., et al. 1998, Proc. SPIE, 3357, 319
Kurk, J. D., Walter, F., Fan, X., et al. 2007, ApJ, 669, 32
Leipski, C., Meisenheimer, K., Walter, F., et al. 2013, ApJ, 772, 103
Lentati, L., Carilli, C., Alexander, P., et al. 2013, MNRAS, 430, 2454
Li, Y., Hernquist, L., Robertson, B., et al. 2007, ApJL, 665, L187
Luhman, M. L., Satyapal, S., Fischer, J., et al. 2003, ApJ, 594, 758
Maiolino, R., Caselli, P., Nagao, T., et al. 2009, A&A, 500, L1
Maiolino, R., Cox, P., Caselli, P., et al. 2005, A&A, 440, L51
Maiolino, R., Gallerani, S., Neri, R., et al. 2012, MNRAS, 425, L66
Maiolino, R., Schneider, R., Oliva, E., et al. 2004, Natur, 431, 533
Malhotra, S., Kaufman, M. J., Hollenbach, D., et al. 2001, ApJ, 561, 766
Marconi, A., & Hunt, L. K. 2003, ApJL, 589, L21
Marsden, G., Borys, C., Chapman, S. C., Halpern, M., & Scott, D. 2005, MNRAS, 359, 43
Morganson, E., De Rosa, G., Decarli, R., et al. 2012, AJ, 143, 142
Mortlock, D. J., Patel, M., Warren, S. J., et al. 2009, A&A, 509, 97
Mortlock, D. J., Warren, S. J., Venemans, B. P., et al. 2011, Natur, 474, 616
Narayanan, D., Li, Y., Cox, T. J., et al. 2008, ApJS, 174, 13
Omont, A., Beelen, A., Bertoldi, F., et al. 2003, A&A, 398, 657
Omont, A., McMahon, R. G., Cox, P., et al. 1996, A&A, 315, 1
Omont, A., Willott, C. J., Beelen, A., et al. 2013, A&A, 552, A43
Petric, A. O., Carilli, C. L., Bertoldi, F., et al. 2003, AJ, 126, 15
Pety, J., Beelen, A., Cox, P., et al. 2004, A&A, 428, L21
Priddey, R. S., Isaak, K. G., McMahon, R. G., Robson, E. I., & Pearson, C. P. 2003, MNRAS, 344, L74
Priddey, R. S., Ivison, R. J., & Issak, K. G. 2008, MNRAS, 383, 289
Priddey, R. S., & McMahon, R. G. 2001, MNRAS, 324, L17

Riechers, D. A., Bradford, C. M., Clements, D. L., et al. 2013, Natur, 496, 329
Riechers, D. A., Walter, F., Bertoldi, G., et al. 2009, ApJ, 703, 1338
Riechers, D. A., Walter, F., Carilli, C. L., Bertoldi, F., & Momjian, E. 2008, ApJL, 686, L9
Robson, I., Priddey, R. S., Isaak, K. G., & McMahon, R. G. 2004, MNRAS, 351, L29
Runnoe, J. C., Brotherton, M. S., & Shang, Z. 2012a, MNRAS, 422, 478
Runnoe, J. C., Brotherton, M. S., & Shang, Z. 2012b, MNRAS, 427, 1800
Sargsyan, L., Lebouteiller, V., Weedman, D., et al. 2012, ApJ, 755, 171
Solomon, P. M., & Vanden Bout, P. A. 2005, ARA&A, 43, 677
Spergel, D. N., Bean, R., Doré, O., et al. 2007, ApJS, 170, 377
Stacey, G. J., Geis, N., Genzel, R., et al. 1991, ApJ, 373, 423
Stacey, G. J., Hailey-Dunsheath, S., Ferkinhoff, C., et al. 2010, ApJ, 724, 957
Swinbank, A. M., Karim, A., Smail, I., et al. 2012, MNRAS, 427, 1066
Valiante, R., Schneider, R., Maiolino, R., Salvadori, S., & Bianchi, S. 2012, MNRAS, 427, L60
Valtchanov, I., Virdee, J., Ivison, R. J., et al. 2011, MNRAS, 415, 3473
Venemans, B. P., McMahon, R. G., Walter, G., et al. 2012, ApJL, 751, L25
Wagg, J., Wiklind, T., Carilli, C., et al. 2012, ApJL, 752, L30
Walter, F., Bertoldi, F., Carilli, C., et al. 2003, Natur, 424, 406
Walter, F., Carilli, C. L., Bertoldi, F., et al. 2004, ApJL, 615, L17
Walter, F., Riechers, D., Cox, P., et al. 2009, Natur, 457, 699
Wang, R., Carilli, C., Beelen, A., et al. 2007, AJ, 134, 617
Wang, R., Carilli, C., Neri, R., et al. 2010, ApJ, 714, 699
Wang, R., Carilli, C., Wagg, J., et al. 2008, ApJ, 687, 848
Wang, R., Wagg, J., Carilli, C., et al. 2011a, AJ, 142, 101
Wang, R., Wagg, J., Carilli, C., et al. 2011b, ApJL, 739, L34
Willott, C. J., Albert, L., Arzoumanian, D., et al. 2010, AJ, 140, 546
Willott, C. J., Delorme, P., Omont, A., et al. 2007, AJ, 134, 2435
Willott, C. J., Delorme, P., Reylé, C., et al. 2009, AJ, 137, 3541
Willott, C. J., Omont, A., & Bergeron, J. 2013, ApJ, 770, 13
Zylka, R. 1998, MOPSI Users Manual (Grenoble: IRAM)